<sup>1</sup>Mihira Kumar Nath <sup>2\*</sup>Sushil Kumar Bhoi <sup>3</sup>Asini Kumar Baliarsingh

# MPPT of PV System under Partial Shading Conditions for SRM Driven Water Pumping Applications Using Pufferfish Optimization



Abstract: - WPSs are necessary for drinking water, agriculture, and industry. A locally installed standby PV-powered WPS is often the finest water supply option. Multiple WPS devices may be required to accommodate demand. This research examines two WPSs supplied by a common PV system and converter. Electricity is needed to extract underground water. Many properties make switched reluctance motors (SRMs) popular with WPSs. The research explores a PV-powered switching reluctance motor (SRM) in a WPS without a battery bank to save money and maintenance. SRM speed is controlled using a sliding mode

Keywords: WPS, MPPT, PV, SRM, Sliding Mode, MRAC, Pufferfish Optimization, Water Pumping.

#### I. INTRODUCTION

Water pumps are essential to industry, agriculture, and drinking. Water resources are crucial to agricultural efficiency, especially in summer when water is scarce. Human consumption and industry need a consistent supply of water, as does agriculture. The needs of WPS require a lot of energy or electricity. PV technology allows us to convert solar energy into electricity in summer [1].

Solar-powered pumps reduce carbon dioxide emissions and operate quietly [2-3]. Solar water pumps are becoming more popular in rural and distant areas since they don't need electrical motors or diesel generators. PV-based WPSs are growing in numerous nations. These maintenance-free alternatives are affordable [4]. However, vast agricultural districts require numerous WPSs for water distribution. The model costs extra since each system includes converters. To fix this, use a converter-PV system with two identical SRMs to operate two WPSs. Overall, SRMs help WPS [5]. This device costs more and is bigger [6]. Thus, single-stage PV-powered WPSs are compact and cost-effective [6-7]. Many research has suggested PV-based WPSs utilizing AC motors, although SRMs are superior [5]. Researchers utilize P&O for MPP identification since it's simple and efficient [2-3, 8]. PV units usually have multiple modules with various PV cells in series and parallel. PV systems may be shaded by dust, plants, buildings, birds, and clouds [6, 9-10]

Pufferfish Optimization Algorithm (POA) is a common GM point identification optimization algorithm [11]. The hybrid POA-P&O (POPO) approach for PSC MPP monitoring is described here. For PSC system performance improvement, the POPO algorithm is compared to three established methods: GA, PSO, MGWO.

A good converter controller is needed for eight or six pole SRM efficiency. The underwater motor-pump setup makes installing a speed sensor tricky and costly. Therefore, this article suggests a speed sensor less controller. SMCs match motor speed to PV power. To regulate motor speed, Figure 1's DC-link control (DCLC) section adjusts the converter's dc-link voltage to POPO's reference value. The Takagi-Sugeno Fuzzy (TS-Fuzzy) controller manages motor speed better than the PI controller during fast irradiance variations [16]. TS-Fuzzy controls adjust SRM speed.

# II. SYSTEM DESCRIPTION

Figure 1 shows a pumping system with a PV unit, a converter, two SRMs, and a new converter controller. Motors will be submerged in water because of submersible pumps. Thus, motor speed is difficult to measure during operation. Using mathematical calculations, a sensor less speed control (SSC) and an SMC have been constructed to regulate the dc-link voltage and produce a reference speed signal for the SRMs. The details of the painstakingly made and designed pieces are below.

<sup>&</sup>lt;sup>1</sup> \*Assistant Professor, Department of Electrical Engineering, Government College of Engineering, Kalahandi, Odisha, India, E-mail: sushilkumarbhoi@gmail.com (Corresponding Author)

<sup>&</sup>lt;sup>2</sup> Assistant Professor, Department of Electrical Engineering, Government College of Engineering, Kalahandi, Odisha, India, E-mail: mihirnath.83@gmail.com

<sup>&</sup>lt;sup>3</sup> Associate Professor, Department of Electrical Engineering, Government College of Engineering, Kalahandi, Odisha, India, E-mail: asinikumar333@gmail.com

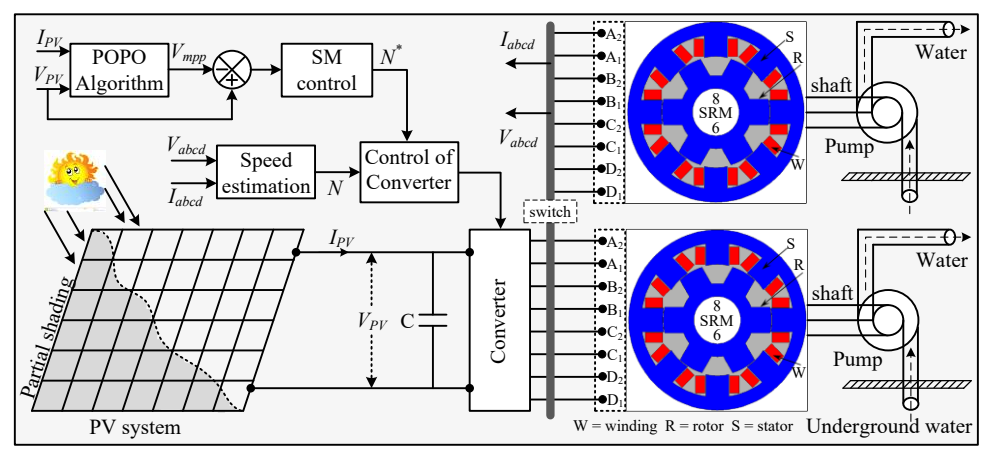


Figure 1: PV fed WPS driven by multiple SRMs.

The breakaway torque (Tb) of a motor or pump typically ranges from (5%-30%) of the maximum torque. The water delivery begins when the pump's velocity attains a baseline threshold ( $\omega$ t). Equation (1) indicates that motor speed influences water flow (Q, gal/min) [9]. Equation (2) illustrates the nonlinear dynamics of the system's head.

$$Q = \begin{cases} x_1 \omega - x_2 & (\omega \ge \omega_t) \\ 0 & (\omega < \omega_t) \end{cases}$$
(1)

$$H = (x_3 \omega^2 + x_4 \omega Q + x_5 Q^2)$$
 (2)

It involves determining a motor's horsepower needs.

$$W_{hp} = \frac{Q \times H}{3960} \tag{3}$$

The constants are x1 to x5. The required horsepower is Whp, while the total head, measured in feet, is symbolized by 'H'.

The energy required to operate the pump must be greater than the Whp.

$$BHP = \frac{W_{hp}}{\text{efficincy of (drive} \times \text{pump)}}$$
(4)

Considering  $Q_{max}$  to be 150 gal/minute, Considering H to be 50 meters, unit pump efficiency, and drive efficiency of 0.94, equation (4) yields 4876 watts as the maximum BHP. From maximum speed and power specs, SRM(s)' load torque is calculated at TL = 25. 0Nm.PV System [5, 15-20] Two PV panels linked in parallel provide 2x4800W of electricity. PV module specifications as follows.

Table-1: Standard values of PV modules

S.No	Parameter	Value
1	Maximum power of each module.	302
2	Short circuit current.	8.16
3	Open circuit voltage.	48.50
4	PV arrays connected in parallel.	2
5	Voltage when the Power is maximum	39.60
6	Current when the power is maximum	7.66
7	Series modules/array.	16

A total of 32 PV modules were integrated into the WPS, with 16 modules arranged in series to attain the necessary rated power and voltage at DC link. Furthermore, two PV arrays were linked in parallel. The voltage associated with the MPP can be monitored through the traditional P&O methodology, which is mathematically defined for consistent solar irradiance.

$$V_{mpp}(t+1) = V_{mpp}(t) + \Delta V \times \text{sign of}\left(\frac{dP_{pv}}{dV_{pv}}\right)$$
(5)

Researchers are interested in the POA because it converges faster than GA, PSO, and MGWO. Adding P&O to the POA may help PV systems under PSC reach MPP.

Table-2: Configuration of PSCs

Patterns	Irradiance level of modules in each array		
PSC-1	PV Panels: 1-3: 1000 W/m <sup>2</sup> , 4-9: 930 W/m <sup>2</sup> , 10-12: 800 W/m <sup>2</sup> , 13-16: 710 W/m <sup>2</sup> .		
PSC-2	PV Panels: 1-4: 990 W/m <sup>2</sup> , 5-7: 920 W/m <sup>2</sup> , 8-13: 780 W/m <sup>2</sup> , 14-16: 590 W/m <sup>2</sup> .		
PSC-3	PV Panels: 1: 820 W/m <sup>2</sup> , 2-3: 730 W/m <sup>2</sup> , 4-11: 520 W/m <sup>2</sup> , 12-16: 350 W/m <sup>2</sup> . 0		

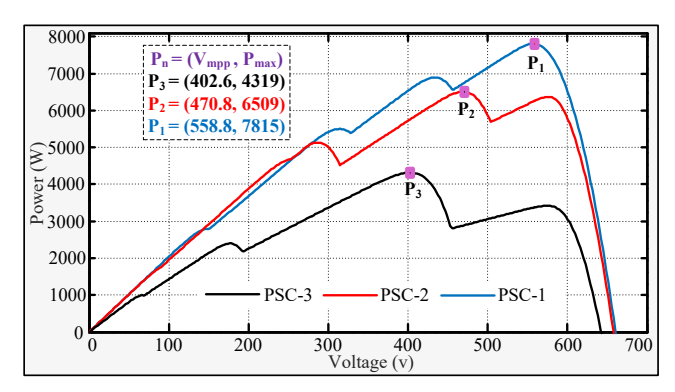


Figure 2: P-V curves as per Table-2.

Dynamics of extra pipe.

The Hazen-Williams algorithm may be used to determine head losses. The incorporation of an extra pipe at the pump outlet is essential for the effective transfer of water between different locations.

$$h_l = 0.002083 \times L \times \left(\frac{Q^{1.85}}{d^{4.8655}}\right) \times \left(\frac{100}{C}\right)^{1.85}$$
(6)

Similarly, the energy loss resulting from the additional piping can be expressed as.

$$\frac{p_a}{\gamma} + \frac{v_1^2}{2g} + Q_{in} = \frac{p_b}{\gamma} + \frac{v_2^2}{2g} + Q_{out} + h_l \tag{7}$$

If the pipe is horizontal: Qin = Qout and v1=v2.

Hence,

$$h_l = \frac{(p_a - p_b)}{\gamma} \tag{8}$$

The length of the extra pipe 'L', the diameter of the pipe 'd', and the friction coefficient 'C' all affect the head loss resulting from the flow resistance of water, hl. Pa and Pb respectively show the forces at the entrance and exit of the additional pipe during the water flow. Denoted as v1 and v2 respectively, the beginning and ultimate velocity of water inside the pipe are respectively The letter "g" represents gravitational acceleration; the density of water is given as " "."

# III. PROPOSED ALGORITHM

The POA is an innovative bio-inspired metaheuristic algorithm that is based on the natural behaviors exhibited by Pufferfish [11].

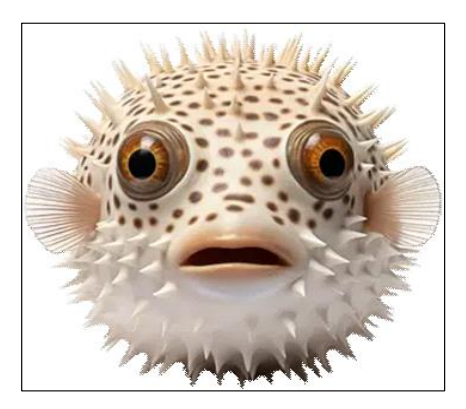


Figure 3: Defensive mode of Pufferfish.

We simulated and compared the POA-associated MPPT approach to many current methods to evaluate its efficacy. The POA outperforms existing methods in convergence speed, accuracy, and robustness. The PV unit MPPT POA mechanism is established next. The vectors present in the community can be expressed mathematically through a matrix, as outlined in Equation (9). The starting position of each member of the POA is determined by Equation (10) at the commencement of the algorithm. Where F is represents voltage point.

$$F = \begin{bmatrix} F_{1,l} & \cdots & F_{1,d} & \cdots & F_{1,m} \\ \vdots & \vdots & & \vdots \\ F_{i,l} & \cdots & F_{i,d} & \cdots & F_{i,m} \\ \vdots & & \vdots & & \vdots \\ F_{n,l} & \cdots & F_{n,d} & \cdots & F_{n,m} \end{bmatrix}$$

$$F_{i,d} = v_{lb} + r \cdot (v_{ub} - v_{lb})$$

$$P_{max} = \begin{bmatrix} P(F_1) \\ \vdots \\ P(F_i) \\ \vdots \\ P(F_n) \end{bmatrix}$$

$$(11)$$

Phase-1: Examination of Predator Assault on Pufferfish (Investigation Stage). Using a simulation of the predator attack strategy targeted at the Pufferfish, which may be stated in the preliminary phase (Phase-1) of the POA, the locations of the population members are reviewed in (12).

$$F_{i,j}^{P1} = F_{i,j} + r_{i,j} \cdot \left( SF_{i,j} - L_{i,j} \cdot F_{i,j} \right)$$
(12)

Phase 2: The Defensive Strategy of Pufferfish against Predators (Exploitation Phase). Under this stage of the Plan of Action, people's positions within the population are reevaluated by simulating the defensive strategies used by a Pufferfish in reaction to predator assaults, as seen below.

$$F_{i,j}^{P2} = F_{i,j} + 1 - 2r_{i,j} \cdot \frac{v_{ub} - v_{lb}}{t}$$
(13)

In this context, V is the population matrix and P is the vector for the assessed objective function. The random number is denoted as r, while vub and vlb signify the upper and lower voltage limits of the PV system, respectively.  $F^{P1,2}$ 

 $F_{i,j}^{P1,2}$  represents the updated arrangement of voltages in relation to their respective phases. The term SFi,j denotes the chosen Pufferfish.

The implementation of the TS-Fuzzy controller utilizes mathematical expressions to define the membership functions for the voltage error ( $^{V_i}$ ) and its derivative ( $^{\dot{V_i}}$ ) signals, which can be categorized into positive (P) and negative (N) values.

The TS-Fuzzy controller employs mathematical formulations to establish the membership functions for the voltage error ( $V_i$ ) and its derivatives ( $\dot{V}_i$ ), applicable to both positive and negative scenarios.

$$\mu_{P}(V_{i}) = \begin{cases} Zero, & (V_{i} < L_{1}) \\ \frac{(V_{i} + L_{1})}{2L_{1}}, & (-L_{1} \leq V_{i} \leq L_{1}) \text{ and} \\ One, & (V_{i} > L_{1}) \end{cases}$$

$$\mu_{N}(V_{i}) = \begin{cases} One, & (V_{i} < L_{1}) \\ \frac{(-V_{i} + L_{1})}{2L_{1}}, & (-L_{1} \leq V_{i} \leq L_{1}) \\ Zero, & V_{i} > L_{1} \end{cases}$$

$$\mu_{P}(\dot{V}_{i}) = \begin{cases} Zero, & (\dot{V}_{i} < L_{2}) \\ \frac{(\dot{V}_{i} + L_{2})}{2L_{2}}, & (-L_{2} \leq \dot{V}_{i} \leq L_{2}) \text{ and} \\ One, & (\dot{V}_{i} > L_{2}) \end{cases}$$

$$\mu_{N}(\dot{V}_{i}) = \begin{cases} One, & (\dot{V}_{i} < L_{2}) \\ \frac{(-\dot{V}_{i} + L_{2})}{2L_{2}}, & (-L_{2} \leq \dot{V}_{i} \leq L_{2}) \\ Zero, & (\dot{V}_{i} > L_{2}) \end{cases}$$

$$(15)$$

Table-3: The TS-fuzzy controller rules:

Rules	Error $V_i(\mathbf{k})$	$\dot{V}_i(\mathbf{k})$	Values
A	Negative	Negative	$(Z_1) = d_1 V_i(\mathbf{k}) + d_2 \dot{V}_i(\mathbf{k})$
В	Negative	Positive	$(Z_2) = \mathbf{d}_3 \times Z_1)$
С	Positive	Negative	$(Z_3) = \mathbf{d}_4 \times Z_1$
D	Positive	Positive	$(Z_4) = \mathbf{d}_5 \times Z_1$

Table-3 contains thorough guidelines on the TS-Fuzzy controller rules. While the rules Z1 to 4 indicate the results of the T-S Fuzzy controller with k representing the sampling moment, it is essential to change the parameters used in TS-Fuzzy. The fuzzy constants d1to5 call for exact modification. By use of a generalized defuzzifier, the TS-Fuzzy (Y) output value is computed by (16).

$$Y = \frac{\sum_{i=1}^{4} Z_i \times B_i}{\sum_{i=1}^{4} Z_i}$$

$$\tag{16}$$

#### IV. PROPOSED CONTROLLER

Water extraction sometimes needs two or more engines. In these cases, a converter-operated multi-motor system and energy management and control methods are essential. Figure 4 shows the WPS control mechanism that works, as described in Figure 1. Figure 4 shows sensor less speed estimate, the DCLC, and SRM DTC in the proposed control approach. Figure 5 shows the SMC's complete internal block diagram, modelled using the equations below.

$$\psi_d = A1 - (B1 + C1 - D1) * \sqrt{2} / 2$$
(17)

$$\psi_q = A1 + B1 - (C1 + D1) * 1/\sqrt{2}$$
(18)

The determination to activate or deactivate the connection of SRM-2 to the converter is based on the power output produced by the PV system. The switch is designed to engage when the PV power attains 4800 W and will automatically deactivate when the power falls to 1900 W, thereby ensuring that two motors do not operate below the critical speed of 720 RPM.

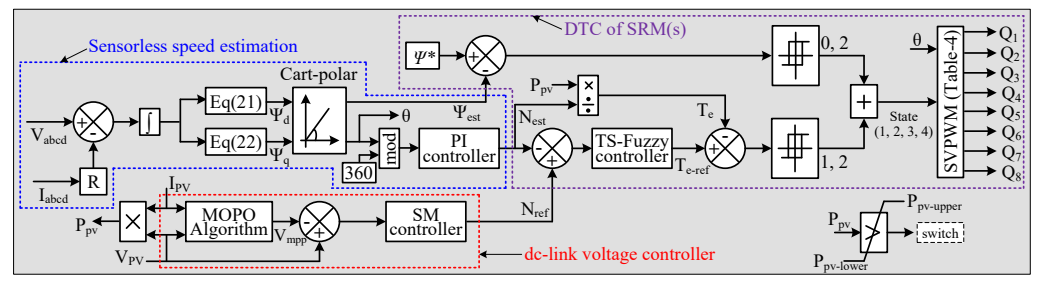


Figure 4: Proposed controller.

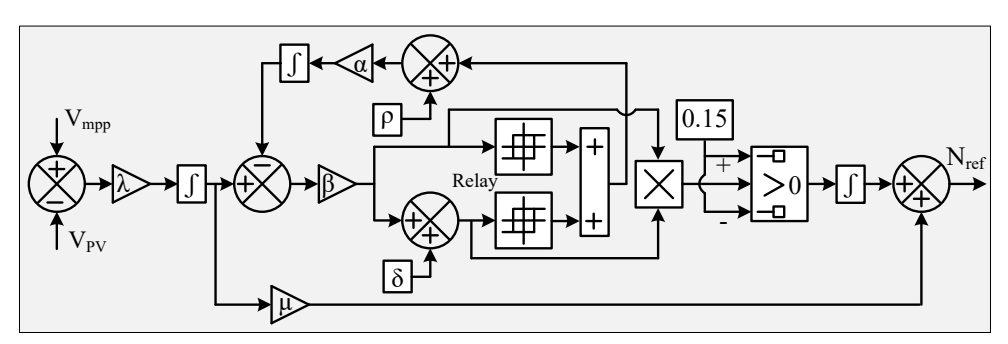


Figure 5: SMC block diagram.

#### V. RESULTS AND DISCUSSION

This research used a real-time simulator (RTS) to test its controllers, which were shown on OPAL-RT. The RTS mimics the PV-based WPS that uses SRM and the recommended control method. Reference [9] provides RTS information. They used two OPAL-RT devices and their computer system to set up Hardware-In-Loop (HIL). As shown in Figure 1, one unit operated the WPS with the PV, converter, SRMs, and pumps, while the other implemented the model's controllers. Figure 6 shows HIL with OPAL RT devices.

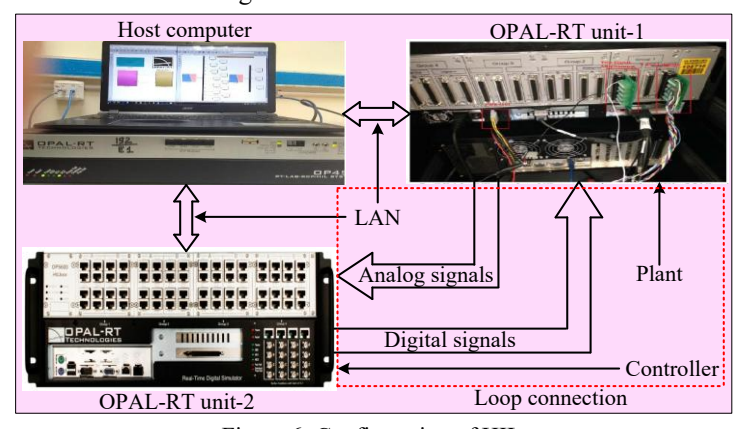


Figure 6: Configuration of HIL.

Analogue signals are sent from the WPS dynamic unit (OPAL RT1) to the control unit (OPAL RT2), while digital signals are sent from the controller to the WPS. OPAL-RT-1 and OPAL-RT-2 form an HIL link using authentic digital and analogue signals.

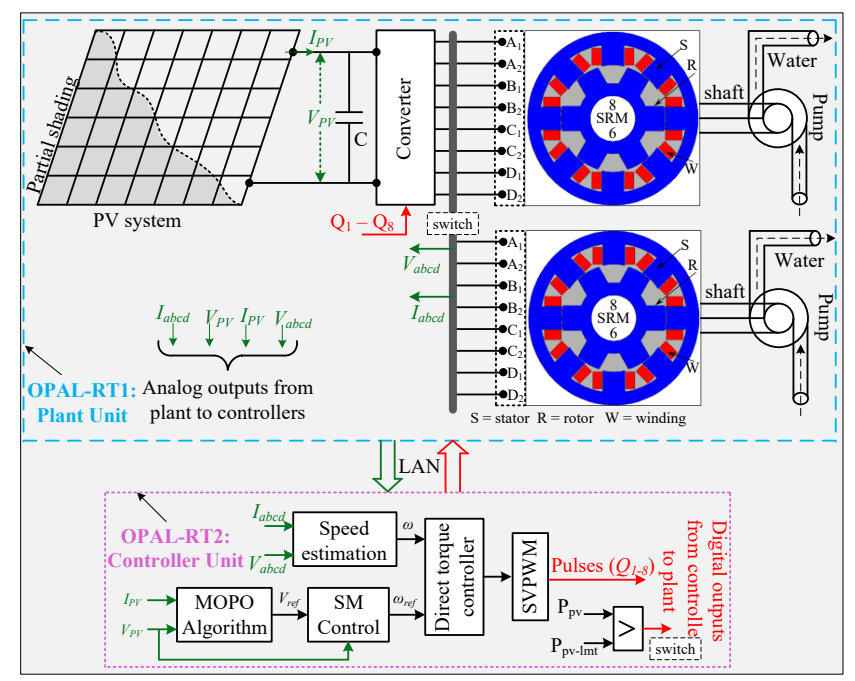


Figure 7: HIL implementation of WPS.

# Case-1: Response of PV under PI and SMC.

In this situation, a variation in solar irradiance from 1000 to 750  $W/m^2$  is being examined at t=3.0 seconds. The assessment of DCLC's performance is conducted through the application of both PI and SMC, as demonstrated in Figure 5. The optimization of the PI gains is tailored for an irradiance level of 1000  $W/m^2$ .

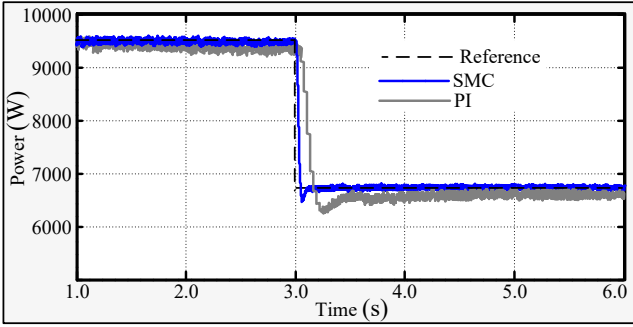


Figure 8: Powers.

# Case-2: Performance among various optimizations.

The main challenge involves enhancing power output in PV systems under PSC. A new hybrid POPO algorithm has been created and evaluated in comparison to PSO, GA, and MGWO algorithms, each of which has been integrated with the P&O mechanism for different PSC scenarios as detailed in Table-2.

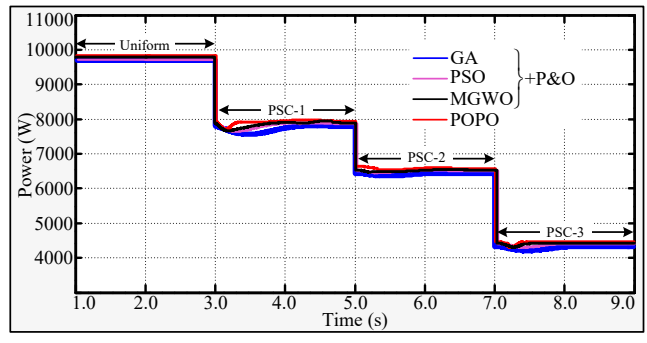


Figure 9: Various powers.

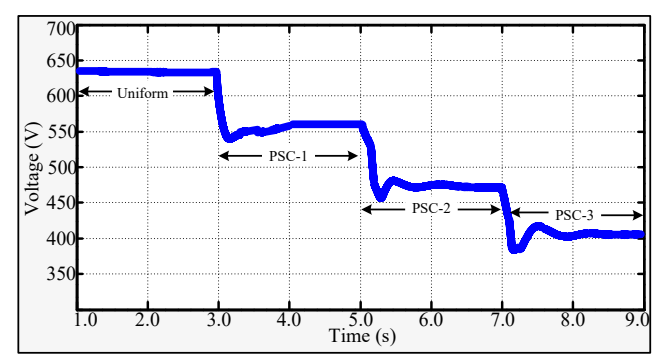


Figure 10: Voltage with POPO.

The bar chart presented in Figure 11 depicts the comparisons for tracking responses of the PV unit under PSCs. The suggested hybrid POPO algorithm demonstrates considerable advantages and exhibits superior performance during PSC when compared to PSO, GA, and MGWO. This is attributed to its capacity to rapidly monitor Vmpp in comparison to alternative optimization methods.

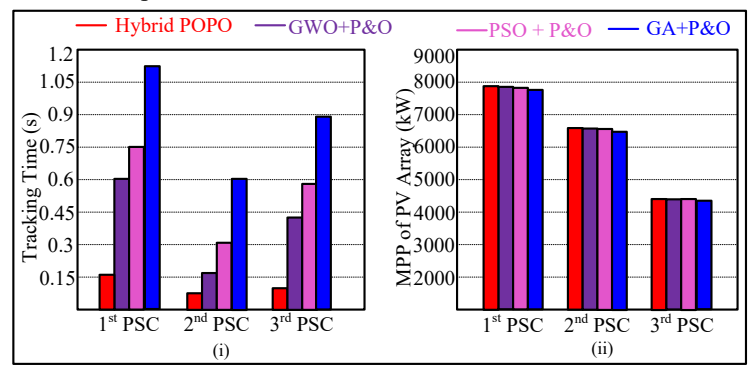


Figure 11: Comparisons.

## Case-3: Under the operation of two SRMs.

Under low irradiation, the PV unit can power one SRM. Mornings, evenings, and considerable partial shade diminish PV system energy production. These cases use one SRM. When the power reaches its maximum threshold (PPV-upper in Figure 4), a switch connects the second SRM to the converter. Increased irradiance establishes this link.

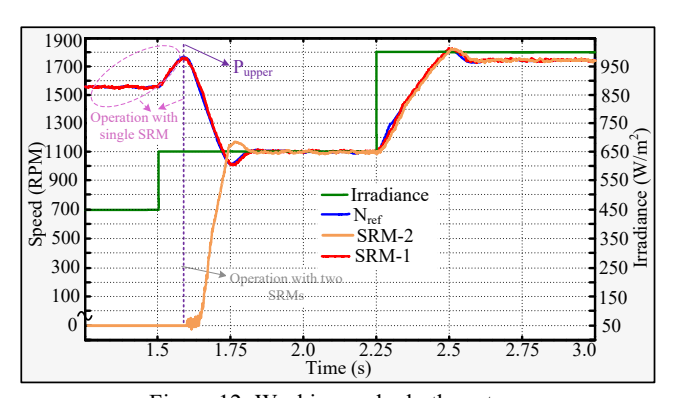


Figure 12: Working under both motors.

# Case-4: Working with an extra pipe

In WPSs, it is customary to incorporate an additional pipe to facilitate the transfer of water from one location to another. Generally, pipes made of PVC, HDPE, Lateral, and LDPE are employed for this application. The torque increases as the length of the pipe extends due to the friction and external forces exerted on the water within the pipe.

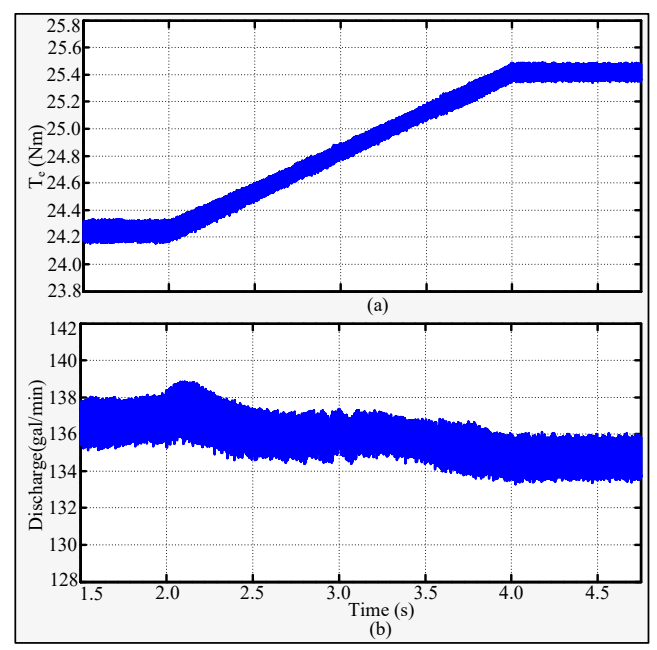


Figure 13: Responses of (a) torque (b) discharge.

The motor torque increases until water reaches the new outlet after an additional bore well pipe is installed. Figures 13 (a) and (b) illustrate the torque and water discharge from a 20-meter pipe bringing water from the bore well exit to the required point. While power output stays constant, motor speed lowers as torque rises. Water flow therefore is constant while the pipe is horizontal. Water discharge may be considerably lowered by friction and outside elements resisting the power and torque of the engine

#### VI. CONCLUSION

Supported by SMC and DTC integration, the SSC SRM-powered PSC fed by PV employs the hybrid POPO algorithm. Under PSCs in a PV unit, the proposed method is evaluated in relation to PSO, GA, and MGWO in MPPT tracking. The OPAL-RT platform shows the findings of actual situations. Built was SMC-based DCLC for quick voltage tracking at dc-link. SMC could modify output to meet the MPP unlike the PI. Emphasizing the need to choose WPS within PSC, the model also handles pragmatic concerns as evaluating SRM load torque and adding extra water transportation pipelines. using the OPAL-RT system.

### REFERENCES

- [1] Bhoi, Sushil Kumar, Kumari Kasturi, and Manas Ranjan Nayak. "Optimisation of the operation of a microgrid with renewable energy sources and battery storage." e-Prime-Advances in Electrical Engineering, Electronics and Energy 4 (2023): 100159.
- [2] Malla, Siva Ganesh, Malla, Jagan Mohana Rao, Malla, Priyanka, Ramasamy, Sreekanth, Doniparthi, Satish Kumar, Sahu, Manoj Kumar, Subudhi, Pravat Kumar and Awad, Hilmy. "Coordinated power management and control of renewable energy sources based smart grid" International Journal of Emerging Electric Power Systems, vol. 23, no. 2, 2022, pp. 261-276. https://doi.org/10.1515/ijeeps-2021-0113
- [3] T. Anuradha et al., "Power Quality Improvement of Hybrid Standalone Microgrid with DSTATCOM during Faults on Distribution Line," 2022 IEEE International Conference on Power Electronics, Drives and Energy Systems (PEDES), Jaipur, India, 2022, pp. 1-7, doi: 10.1109/PEDES56012.2022.10080027.
- [4] D. Vannurappa, G. P. R. Reddy, K. Deepak, Y. Hazarathaiah, S. S. Prasad and S. G. Malla, "Small Signal Analysis of Photovoltaic based Water-Pumping System Driven by Induction Motor," 2023 7th International Conference on Computing Methodologies and Communication (ICCMC), Erode, India, 2023, pp. 15-20, doi: 10.1109/ICCMC56507.2023.10083929.
- [5] P. Bellamkonda et al., "Modified Grey Wolf Optimization Algorithm for PV Fed Water Pumping System Driven by Switched Reluctance Motor under Partial Shading Condition," 2022 IEEE International Conference on Power Electronics, Drives and Energy Systems (PEDES), Jaipur, India, 2022, pp. 1-6, doi: 10.1109/PEDES56012.2022.10080719.
- [6] Malla, S.G., Malla, P., Karthik, M. et al. Modified Invasive Weed Optimization for the Control of Photovoltaic Powered Induction Motor Drives in Water Pumping Systems. Iran J Sci Technol Trans Electr Eng 47, 925–938 (2023). https://doi.org/10.1007/s40998-023-00589-7.

- [7] V M Revathi and K Subramani and S Krishnakumar and Ahmed Hussein Alawadi and R Senthil Kumar and Siva Ganesh Malla, "A modified invasive weed optimization for MPPT of PV based water pumping system driven by induction motor", IOP: Engineering Research Express, volume 6, number 3, July 2024, https://dx.doi.org/10.1088/2631-8695/ad5cd3.
- [8] Kandi Bhanu Prakash, "Modeling of DC to DC Converter for Renewable Energy Sources", International Journal of New Technologies in Science and Engineering (IJNTSE), Vol. 9, Issue. 1, pp. 6-10, Jan. 2023.
- [9] S. G. Malla et al., "Whale Optimization Algorithm for PV Based Water Pumping System Driven by BLDC Motor Using Sliding Mode Controller," in IEEE Journal of Emerging and Selected Topics in Power Electronics, vol. 10, no. 4, pp. 4832-4844, Aug. 2022, doi: 10.1109/JESTPE.2022.3150008.
- [10] M. B. Lakshmi et al., "Voltage and Frequency Control of a PV-Battery-Diesel Generator based Standalone Hybrid System," 2022 IEEE International Conference on Power Electronics, Drives and Energy Systems (PEDES), Jaipur, India, 2022, pp. 1-7, doi: 10.1109/PEDES56012.2022.10080764.
- [11] Al-Baik, O.; Alomari, S.; Alssayed, O.; Gochhait, S.; Leonova, I.; Dutta, U.; Malik, O.P.; Montazeri, Z.; Dehghani, M. Pufferfish Optimization Algorithm: A New Bio-Inspired Metaheuristic Algorithm for Solving Optimization Problems. Biomimetics 2024, 9, 65. https://doi.org/10.3390/biomimetics9020065.
- [12] M. Muddhey, R. K. Behera and U. R. Muduli, "Solar PV and Battery Assisted Isolated Power Supply Control and Implementation," 2022 IEEE International Conference on Power Electronics, Drives and Energy Systems (PEDES), Jaipur, India, 2022, pp. 1-5, doi: 10.1109/PEDES56012.2022.10080581.
- [13] S. Prakash, O. A. Zaabi, R. K. Behera, K. A. Jaafari, K. A. Hosani and U. R. Muduli, "Modeling and Dynamic Stability Analysis of the Grid-Following Inverter Integrated With Photovoltaics," in IEEE Journal of Emerging and Selected Topics in Power Electronics, vol. 11, no. 4, pp. 3788-3802, Aug. 2023, doi: 10.1109/JESTPE.2023.3272822.
- [14] D. Fares, M. Fathi and S. Mekhilef, "Comparison of Two Hybrid Global Maximum Power Point Algorithms for Photovoltaic Module Under Both Uniform and Partial Shading Condition," 2020 International Conference on Electrical, Communication, and Computer Engineering (ICECCE), Istanbul, Turkey, 2020, pp. 1-6, doi: 10.1109/ICECCE49384.2020.9179426.
- [15] R. Sangrody, S. Taheri, A. -M. Cretu and E. Pouresmaeil, "An Improved PSO-Based MPPT Technique Using Stability and Steady State Analyses Under Partial Shading Conditions," in IEEE Transactions on Sustainable Energy, vol. 15, no. 1, pp. 136-145, Jan. 2024, doi: 10.1109/TSTE.2023.3274939.
- [16] Mansour Aljohani, Siva Ganesh Malla and Mohamed I. Mosaad, TS-Fuzzy Controllers based Novel Control of Grid Connected Fuel Cell Stack System, E3S Web of Conf., Volume 540, 2024, https://doi.org/10.1051/e3sconf/202454010005.
- [17] S. K. Baksi, R. K. Behera and U. R. Muduli, "A new Transformerless Five-level Boost Inverter with Minimum Switch Count For Photovoltaic Application," 2023 IEEE 3rd International Conference on Smart Technologies for Power, Energy and Control (STPEC), Bhubaneswar, India, 2023, pp. 1-6, doi: 10.1109/STPEC59253.2023.10430976.
- [18] S. K. Baksi, R. K. Behera and U. R. Muduli, "Comprehensive Overview of Reduced Switch Count Multilevel Inverter for PV Applications," 2023 IEEE 3rd International Conference on Smart Technologies for Power, Energy and Control (STPEC), Bhubaneswar, India, 2023, pp. 1-6, doi: 10.1109/STPEC59253.2023.10431075.
- [19] Bhoi, Sushil Kumar, and Manas Ranjan Nayak. "Optimal scheduling of battery storage with grid tied PV systems for trade-off between consumer energy cost and storage health." Microprocessors and Microsystems 79 (2020): 103274.
- [20] S. K. Baksi, R. K. Behera and U. R. Muduli, "Optimized 9-Level Switched-Capacitor Inverter for Grid-Connected Photovoltaic Systems," in IEEE Transactions on Industry Applications, vol. 60, no. 2, pp. 3284-3296, March-April 2024, doi: 10.1109/TIA.2023.3332059.